A Cheap and Easy Method for 3D C-arm Reconstruction using Elliptic Curves

David Burkhardt[a], Ameet Jain[b], Gabor Fichtinger[b]

[a]Haverford College
[b]Johns Hopkins University

ABSTRACT

For quantitative C-arm fluoroscopy, we had earlier proposed a unified mathematical framework to tackle the issues of pose estimation, correspondence and reconstruction, without the use of external trackers. The method used randomly distributed unknown points in the imaging volume, either naturally present or induced by placing beads on the patient. These points were then inputted to an algorithm that computed the 3D reconstruction. The algorithm had an 8° region of convergence, which in general could be considered sufficient for most applications. Here, we extend the earlier algorithm to make it more robust and clinically acceptable. We propose the use of a circle/ellipse, naturally found in many images. We show that the projection of elliptic curves constrain 5 out of the 6 degrees of freedom of the C-arm pose. To completely recover the true C-arm pose, we use constraints in the form of point correspondences between the images. We provide an algorithm to easily obtain a virtual correspondence across all the images and show that two correspondences can recover the true pose 95% of the time when the seeds employed are separated by a distance of 40 mm. or greater. Phantom experiments across three images indicate a pose estimation accuracy of 1.7° using an ellipse and two sufficiently separated point correspondences. Average execution time in this case is 130 seconds. The method appears to be sufficiently accurate for clinical applications and does not require any significant modification of clinical protocol.

Keywords: Tracking, Localization, Registration, X-ray reconstruction, C-arm pose estimation

1. INTRODUCTION

With an approximate annual incidence of 220,000 new cases and 33,000 deaths prostate cancer continues to be the most common cancer in men in the United States.[1] For several decades, the definitive treatment for low risk prostate cancer was radical prostatectomy or external beam radiation therapy,[2] but low dose rate permanent seed brachytherapy (shortly brachytherapy thereafter in this document) today can achieve virtually equivalent outcomes.[3,4] The success of brachytherapy chiefly depends on our ability to tailor the therapeutic dose to the patients individual anatomy. In contemporary practice, however, implant planning is based on idealistic preplanned seed patterns that, as 15 years of clinical practice has clearly demonstrated, are not achievable in the actual human body. According to a comprehensive review by the American Brachytherapy Society,[5] the preplanned technique used for permanent prostate brachytherapy has limitations that may be overcome by intraoperative planning. At the same time, continues the re-port, the major current limitation of intraoperative planning is the inability to localize the seeds in relation to the prostate. There are excellent algorithmic and computational tools available today to optimize a brachytherapy treatment plan intraoperatively, thereby allowing for an improved dose coverage. These methods, however, critically require that the exact three-dimensional locations of the implanted seeds are precisely known with respect to the patients anatomy.

C-arm fluoroscopy is attractive as a means to generate this precise knowledge. It is the most widely used intraoperative imaging modality in general surgery. However, it presently lacks the ability for robust and easy quantitative guidance.

Further author information: (Send correspondence to Ameet Jain)
David Burkhardt: E-mail: dburkhar@haverford.edu
Ameet Jain: E-mail: ajain@cs.jhu.edu
Gabor Fichtinger E-mail: gabor@cs.jhu.edu

Medical Imaging 2007: Visualization and Image-Guided Procedures, edited by Kevin R. Cleary, Michael I. Miga,
Proc. of SPIE Vol. 6509, 65090B, (2007) · 1605-7422/07/$18 · doi: 10.1117/12.712395

Quantitative fluoroscopy-guided surgery needs to solve four major problems: 1 C-arm image distortion; 2 the calibration of imaging parameters; 3 pose recovery or tracking; and 4 registration to imaging modalities. The first two are well-studied problems in the literature.[6–8] In particular, it has been suggested that precise calibration of C-arm parameters do not significantly improve pose reconstruction.[9] Through modeling the effects of mis-calibration as an affine transform, it is demonstrated that C-arm tracking is insensitive to mis-calibrations: mis-calibration of up to 50 mm adds no additional error in 3D reconstruction of small objects. A constant calibration can therefore be assumed for all images. On the other hand, pose recovery on unencoded C-arm machines is a major technical problem that presently does not have a clinically practical solution in many areas of application.

In current commercial C-arm fluoroscopy surgical navigation systems, pose recovery is performed through localizing the x-ray detector in room coordinates by some auxiliary optical tracker[10,11] or electromagnetic EM tracker.[12] Unfortunately, auxiliary trackers sometimes become impractical for various reasons. They are expensive and add to the complexity of the operating room since they require an additional calibration step. Optical trackers require a line of sight, which becomes cumbersome in a clinical setting and requires an alteration in the standard work flow. The EM trackers can successfully overcome this issue, but become susceptible to field distortion from metal objects like surgical tools or the C arm itself, compromising on accuracy.

In a recent publication,[13] the authors delineate the above problems and also say that using optical trackers reduces the useful imaging volume of the fluoroscope and potentially compromises the achievable accuracies. Despite using an optical tracker to track their surgical tools, they explicitly choose to not track the C arm using the tracker but instead use a radio-opaque fiducial. Their system has been fairly successful for various surgeries and has been in clinical use for the last four years. To make the fiducials feasible, recent publications have reported smaller fiducials by compact bead placement. In one study an artificially induced fiducial, consisting of several lines, seeds and ellipses, was demonstrated to be capable of uniquely determining correct C-arm pose with mean accuracy of .33° in rotation and .53 mm in translation.[14]

Solutions that require only objects naturally present in the image frame in the surgery room are more attractive still. In many applications, screw/needle ends, implanted surgical markers, special anatomy points etc. are naturally present in the images. By enforcing the "consistency" of these feature points across the images, one can potentially solve for all unknown parameters of calibration, pose recovery, matching, and reconstruction in one massive high-dimensional non-linear optimization. In particular, in the case of brachytherapy there are many seeds present that may be usable for optimization.

Accurate three dimensional reconstruction of the brachytherapy seeds requires that individual seeds be matched between multiple images. Seed matching can be formalized as a combinatorial optimization problem, and demonstrates that the Hungarian algorithm can be applied to match seeds between images. It is proved that, using the Hungarian algorithm, two images are insufficient to uniquely match seeds. Three images are necessary, and in practice more may be needed for the identification of seeds that are not visible in all images.[15]

Considerable work has been done in studying the usefulness of conic images in image reconstruction, both in segmenting conic curves in images and in determining pose based on successful segmentations.[16–24] It has been demonstrated that images of conics can be used in pose determination. In particular, it is possible to determine, to a single rotational degree of freedom, the pose from which an image was generated based on a single image of a circle within the image frame.[25]

In this paper, we propose a solution to accurately estimate the pose by placing a wire in the shape of an elliptic curve in the imaging frame. We demonstrate that images of this ellipse constrain 5 of the 6 pose reconstruction degrees of freedom. Previously designed algorithms that determine a correspondence between brachytherapy seeds can be used to provide seed correspondences. These correspondences will be combined with a non-linear optimization to determine C-arm pose.

2. METHODS

2.1. Imaging Setup

A C-arm fluoroscope was used to generate three images of an artificial brachytherapy seed cloud to be used to test our ability to reconstruct C-arm pose. A fiducial device that includes two wire ellipses is placed in the

Figure 1. Fiducial device containing wire ellipses, and seed cloud phantom to be used in assessing algorithm. Within the phantom cloud block are precisely positioned sample seeds.

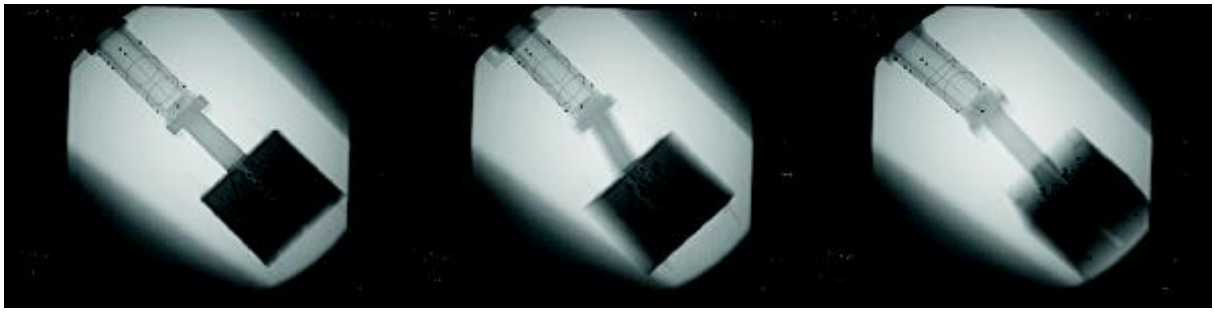

Figure 2. Three sample C-arm Images of a phantom brachytherapy seed cloud and fiducial with ellipse

imaging frame, and is used to create an image of an ellipse in each C-arm image. The design for the fiducial was refined by generating multiple rough prototypes from ABS acrylonitrile butadiene styrene using an FDM fused deposition modeling rapid prototype machine. The final fiducial design was then fabricated from a acetol rod using a four-axis CNC computer numerical control mill. The cylinder was press fit into a custom acetol mount that provided three mutually orthogonal sets of mounting holes for attaching to an accurate rotary table for validation. The dimensions of the ellipse were precisely controlled in its manufacture.

The brachytherapy seed cloud was modeled by a highly precise phantom. Real x-ray images were taken of the phantom using a fluoroscope Philips BV 3000. The system-supplied parameters were read from the DICOM header, otherwise the fluoroscope was not explicitly calibrated. Moreover, the images were not distortion corrected distortion 2 mm. The fiducial was mounted on a highly accurate 0.002° resolution rotational turntable 30000 Heavy Load Worm Gear Drive from Parker Automation, Irwin, Pennsylvania. The fluoroscope remains stationary while the fiducial moves in a known path, providing ground truth. The fiducial with seed cloud phantom attached is shown in Figure 1 A sample set of three images produced by this set-up is presented in Figure 2.

A fiducial mount was designed such that it produced zero translation and a known rotation when the turntable was rotated. The design supported the two independent rotation axes typical to C arms. Thus, given any starting pose, the relative motion between the current pose and the starting pose is known precisely from the turntable reading. The relative motion is also calculated using our algorithm from computed current pose and the computed starting pose. The difference between the computed relative motion and known relative motion is the error.

2.2. Reconstruction Algorithm Design

An algorithm was designed and executed on the C-arm images to reconstruct pose. Previously designed segmentation algorithms were used to determine the location of the ellipse and the brachytherapy seeds in the images. These algorithms produced ellipses equations of the form:

$$Au^2 + Buv + Cu^2 + Du + Fv + G = 0 \tag{1}$$

in each image, in which u and v are respectively the coordinates along the x and y axis of the image, measured in pixels, and A, B, C, D, F, and G are constants determined by the algorithm. This equation and the assumed C-arm calibration can be used to determine the equation of the three dimensional cone which has as vertex the focal point of the X-ray source. This equation will be

$$A_0x^2 + B_0xy + C_0x^2 + \frac{D_0}{f}xz + \frac{F_0}{f}yz + \frac{G_0}{f^2}z^2 = 0. \tag{2}$$

where x, y, z are coordinates in a system that has the focal point of the x-ray device as origin with z axis perpendicular to the image plane and x and y axis parallel to the imaging plane, and f is the focal length of the imaging scenario. This equation can be represented in matrix form as

$$\begin{bmatrix} x & y & z \end{bmatrix} \begin{bmatrix} A_0 & \frac{B_0}{2} & \frac{D_0}{2f} \\ \frac{B_0}{2} & C_0 & \frac{F_0}{2f} \\ \frac{D_0}{2f} & \frac{F_0}{2f} & \frac{G_0}{f^2} \end{bmatrix} \begin{bmatrix} x \\ y \\ z \end{bmatrix} = 0. \tag{3}$$

Given the dimensions of the ellipse, our task was to find the transformation between a coordinate system centered on the physical ellipse with x axis along its major axis and y axis along its minor axis and the system with origin at the imaging focal point and with x axis along the image x axis of the image, y axis along the image y axis of the image, and z axis perpendicular to the image plane.

We broke the process into several steps using a method similar to that described for the case of a circle by Costa and Shapiro.[25] The first step involved finding the rotation between the system of coordinates defined by the image plane, and the system with x and y axes along the major and minor axis of the cone and z axis along the cone's center. This coordinate system is of particular interest because in it the cone equation is of the form:

$$\begin{bmatrix} x & y & z \end{bmatrix} \begin{bmatrix} A_B & 0 & 0 \\ 0 & C_B & 0 \\ 0 & 0 & \frac{G_B}{f^2} \end{bmatrix} \begin{bmatrix} x \\ y \\ z \end{bmatrix} = 0 \tag{4}$$

Having the equation in this form makes it easier to work with in the next step. The rotation matrix that achieves it is just the eigenvectors of the original cone matrix M_0, since multiplying a matrix by one of its eigenvectors and right multiplying by the transpose of that same matrix produced a diagonalized version of the initial matrix.

We next sought to find the transformation between this coordinate system with z axis perpendicular to the cone base and one with z axis perpendicular to the surface of the physical wire ellipse. Through applying constraints imposed by the ellipse, we sought to find the set of transformations that would achieve this for a given image. We parameterized the problem by defining two values, ϕ and θ which together can represent a rotation from the frame with axis aligned with the cone base to any other axis system. The coordinate system is first rotated by ϕ about the z axis of the original coordinate system, then by θ around the new y axis. This relationship is demonstrated in Figure 3 For any image, there are infinitely many possible $\phi - \theta$ combinations, corresponding to infinitely many possible physical ellipses that could generate a given ellipse image. These rotations can be expressed by the following matrices:

$$R_\phi = \begin{bmatrix} cos(\phi) & -sin(\phi) & 0 \\ sin(\phi) & cos(\phi) & 0 \\ 0 & 0 & 1 \end{bmatrix} \tag{5}$$

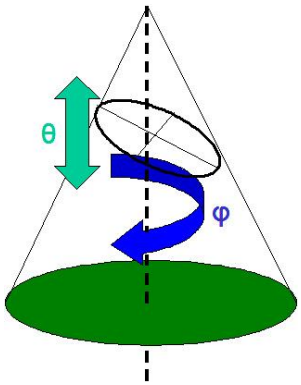

Figure 3. Graphical representation of the angles phi and theta, used in pose reconstruction

$$R_\theta = \begin{bmatrix} cos(\theta) & 0 & sin(\theta) \\ 0 & 1 & 0 \\ -sin(\theta) & 0 & cos(\theta) \end{bmatrix} \tag{6}$$

Our goal therefore is to solve for ϕ and θ such that:

$$X R_\phi R_\theta M_P R_\phi^T R_\theta^T X^T = 0 \tag{7}$$

Where M_P is the equation for the cone in the coordinate system with z axis perpendicular to the actual ellipse. We have several constraints related to this cone that we can put in place to determine the set of $\phi - \theta$ solutions. We know that any plane parallel to the x-y plane will slice the cone in a section with eccentricity equal to the eccentricity of the physical ellipse, and this eccentricity is a known constant. So, if we set Z constant we will get the equation of an ellipse with eccentricity. Doing this gives us:

$$A_P * x^2 + B_P * xy + C_P * y = K \tag{8}$$

$$A_P = G_0 * sin^2(\theta) + C_0 * cos^2(\theta) sin^2(\phi) + A_0 * cos^2(\theta) cos^2(\phi) \tag{9}$$

$$B_P = 2\{-A_0 * cos(\theta) cos(\phi) * sin(\phi) + C_0 * cos(\theta) sin(\phi) cos(\phi)\} \tag{10}$$

$$C_P = A_0 * sin^2(\phi) + C_0 * cos^2(\phi) \tag{11}$$

The ellipse generated in this slice will be described by the equation:

$$\frac{(x * cos(\psi) + y * sin(\psi))^2}{a^2} + \frac{(x * sin(\psi) - y * cos(\psi))^2}{b^2} = K \tag{12}$$

With ψ as some rotation angle, and a and b as the major and minor axes of the real ellipse. K will be some constant dependent on the z value at which the slice was taken Expanding this equation gives us:

$$\left(\frac{cos^2(\psi)}{a^2} + \frac{sin^2(\psi)}{b^2}\right) x^2 + sin(2\psi)\left(\frac{1}{a^2} - \frac{1}{b^2}\right) xy + \left(\frac{sin^2(\psi)}{a^2} + \frac{cos^2(\psi)}{b^2}\right) y^2 = K \tag{13}$$

So, we know that for some angle of rotation ψ:

$$A_P = \left(\frac{cos^2(\psi)}{a^2} + \frac{sin^2(\psi)}{b^2}\right)$$
$$B_P = sin(2\psi)\left(\frac{1}{a^2} - \frac{1}{b^2}\right)$$
$$C_P = \left(\frac{sin^2(\psi)}{a^2} + \frac{cos^2(\psi)}{b^2}\right)$$

We can combine these statements to place a constraint on the allowed values of these constants relative to each other: trigonometric identities allow us to say that:

$$A_P + C_P = K\left(\frac{1}{a^2} + \frac{1}{b^2}\right)$$
$$(A_P - C_P)^2 + B_0^2 = K^2\left(\frac{1}{a^2} - \frac{1}{b^2}\right)^2$$

$$A_P + C_P = K\left(\frac{1}{a^2} + \frac{1}{b^2}\right)$$
$$(A_P - C_P)^2 + B_0^2 = K^2\left(\frac{1}{a^2} - \frac{1}{b^2}\right)^2$$

These can be combined to say that:

$$\frac{(A_P - C_P)^2 + B_P^2}{(A_P + C_P)^2} = \frac{(\frac{b^2}{a^2} - 1)^2}{(\frac{b^2}{a^2} + 1)^2}$$

Substituting the values for A_P, B_P, and C_P previously presented in equations 9, 10, 11 allows us to obtain an equation relating θ to ϕ. This equation is a quadratic equation in $cos^2(\phi)$ of the form:

$$0 = K_1(\theta) * cos^4(\phi) + K_2(\theta) * cos^2(\phi) + K_3(\theta) \tag{14}$$

With the $K_n(\theta)$ functions of θ defined as follows:

$$K_1 = -4 * (-C_P + A_P)^2 * \frac{a}{b} * (1 - 2 * cos(\theta)^2 + cos(\theta)^4)/(\frac{a}{b} + 1)^2 \tag{15}$$

$$K_2 = \frac{(\frac{a}{b} - 1)^2}{(\frac{a}{b} + 1)^2} * (G_P * sin(\theta)^2 + C_P * cos(\theta)^2)^2 + \frac{(\frac{a}{b} - 1)^2}{(\frac{a}{b} + 1)^2} * A_P^2 + 2\frac{(\frac{a}{b} - 1)^2}{(\frac{a}{b} + 1)^2} * (G_P * sin(\theta)^2 +$$
$$C_P * cos(\theta)^2) * A_P - (G_P * sin(\theta)^2 + C_P * cos(\theta)^2)^2 - A_P^2 + (2 * G_P * sin(\theta)^2 + 2 * C1 * cos(\theta)^2) * A_P \tag{16}$$

$$K_3 = -4 * (2 * \frac{a}{b} * G_P * C_P * cos(\theta)^2 - 2 * \frac{a}{b} * G_P * C_P * cos(\theta)^4 - A_P * C_P * cos(\theta)^2 - A_P * G_P$$
$$+ A_P * G_P * cos(\theta)^2 + \frac{a}{b} * C_P^2 * cos(\theta)^4 + a/b * G_P^2 - 2 * \frac{a}{b} * G_P^2 * cos(\theta)^2 + \frac{a}{b} * G_P^2 * cos(\theta)^4$$
$$- A_P * \frac{a}{b^2} * C_P * cos(\theta)^2 - A_P * \frac{a}{b}^2 * G_P + A_P * a/b^2 * G_P * cos(\theta)^2 + A_P^2 * \frac{a}{b})/(\frac{a}{b} + 1)^2 \tag{17}$$

Since 14 is a quadratic equation in $cos^2(\phi)$, for any given value of ϕ there are 4 values of θ that satisfy the constraint that it imposes. After choosing a $\phi - \theta$ combination to consider, we apply these transformations to our coordinate system. This gives us a cone equation of the form:

$$XR_\phi R_\theta M_P R_\phi^T R_\theta^T X^T = XC_E X^T = 0 \tag{18}$$

Where C_E is the cone in a coordinate system with z axis perpendicular to the face of the real ellipse. We next apply a rotation by the angle ψ to bring the x and y axes of our coordinate system parallel to the major and minor axes of the real ellipse. To solve for ψ, we solve for the values that sets B_E to 0. This angle is given by:

$$\psi = 1/2 * atan(2 * B_E/(C_E - A_E)) \tag{19}$$

Transforming the coordinate system by a rotation around the z axis of the angle ψ, which is described by the transformation matrix:

$$\begin{bmatrix} cos(\psi) & -sin(\psi) & 0 & 0 \\ sin(\psi) & cos(\psi) & 0 & 0 \\ 0 & 0 & 1 & 0 \\ 0 & 0 & 0 & 1 \end{bmatrix} \tag{20}$$

The coordinate system created by the combination of these rotations now has axes parallel to the axes of the real ellipse, but is centered at the imaging focal point. The final step in our algorithm is therefore a translation to bring the center of the coordinate system to the center of the ellipse. This translation is computed by taking a slice of the cone a distance f away from the focal points, computing its major axis at this point, and using this computation to determine where on the cone a slice would have major axis equal to the major axis of the actual real ellipse. The coordinate system is then translated by this vector.

Combining these transformations allows us to create an algorithm to determine the set of possible poses that could have created a given image. However, as infinitely many possible $\phi - \theta$ combinations exist, the ellipse image can not be used to uniquely determine the pose. It constrains 5 of the 6 degrees of freedom of pose, allowing a single degree of freedom that must be removed through further constraints.

To constrain this set to a single solution, additional information is necessary. Correspondences between points in the brachytherapy seed cloud can be used to create the necessary additional constraints. We designed an algorithm that could take as input a proposed set of poses and a set of corresponding point images, and determine the actual three-dimensional location of the image points, and the error in point segmentation that this set of poses would imply. By optimizing for minimal projection error, we were able to determine possible poses that might produce the images observed.

3. RESULTS

The algorithm was tested using C-arm images of a phantom brachytherapy seed cloud near a metal ellipse. Initially, trials were run with only one additional point correspondence. This seemed like an attractive possibility since this correspondence could come from the mean location of all segmented seeds and might allow for the seed correspondence step to be bypassed. With only one additional point correspondence, the algorithm succeeded in only 9 of 20 cases, indicating that a single correspondence is insufficient to satisfactorily resolve pose. Sets of 2 and 3 seeds were selected at random, and were used in the optimization function to attempt to reconstruct C-arm pose. Average distance between the points used in optimization was measured and recorded. A sample reconstruction is presented in Figure 4.

With the addition of other point correspondence, the success of the algorithm was shown to depend considerably on the distance between the two points being used. The algorithm was defined to have succeeded if

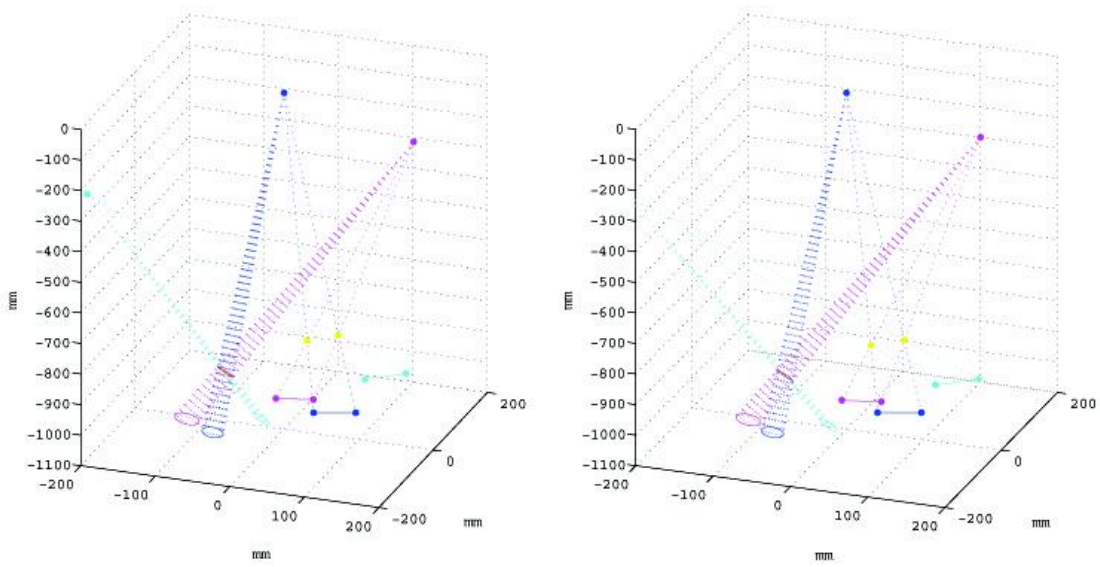

Figure 4. Sample representation of the pose reconstruction from the images presented in Figure 2. On left is the ground truth, while on right is the reconstructed pose. Each of the cone vertices represents an x-ray source, while the cone bases represent ellipse images. The three cones intersect at the location of the real ellipse. The points are points used to generate additional constraints; their images lie in plane with the ellipses to which they correspond

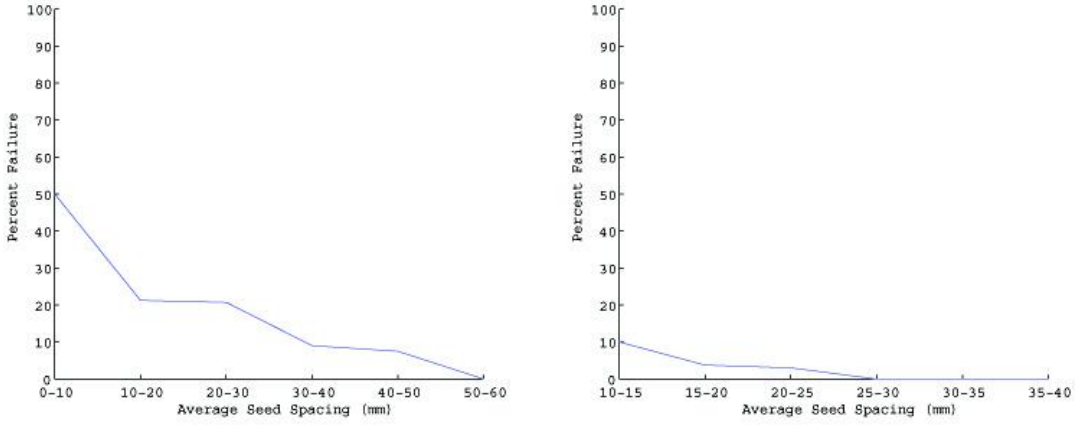

Figure 5. Observed rate of failure. On the left are the results from optimizing using 2 brachytherapy seeds, and on the right are results produced using 3 brachytherapy seeds. X axis is the average spacing between seeds used.spacings

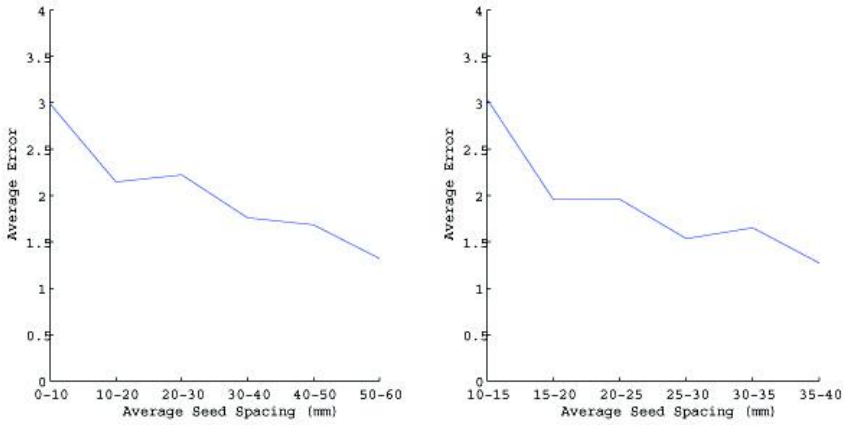

Figure 6. Observed Angular Error in non-failure cases for for 2 and 3 brachytherapy seeds, using sets of seeds with various average spacings

the average error in reconstructed pose as compared with actual pose was less than 7° The rate at which the algorithm was able to successfully reconstruct pose is presented as a function of bead spacing in Figure 5. As this figure demonstrates, for most cases with 2 points, or for cases with 3 points and wide spacing, failure rate becomes quite low. For those cases in which pose was reconstructed, the average angular error still did display some dependence on seed spacing and number of seeds used in reconstruction. This relationship is presented in Figure 6.

4. DISCUSSION

An algorithm has been presented that is capable of determining C-arm pose from three images of a single ellipse and correspondences between additional points. Coupled with previous work that enables point correspondence matching, this algorithm could be applied to reconstruct C-arm pose for three images of a brachytherapy patient, with a single artificially manufactured wire ellipse of known dimension as the only addition to the imaging situation. This represents a significant step toward a complete pose reconstruction system employing no external hardware.

An aim of further work might be to determine the number of point correspondences that should be theoretically required to exactly determine pose. In addition, it would be desirable to include the ellipse into the error calculation process; further work could focus on determining the effective weightings that should be given to the points and to the ellipse in such an error calculation.

REFERENCES

1. A. Jemal, "Cancer statistics," *Ca-Cancer J. Clin* **54**, pp. 8–29, 2004.
2. R. Peschel and J. Coldberg, "Surgery, brachytherapy, and external-beam radiotherapy for early prostate cancer," *Lancet. Oncol.* **4**, pp. 233–241, 2002.
3. G. Merrick, W. Butler, J. Lief, and A. Dorsey, "Is brachytherapy comparable with radical prostatectomy and external-beam radiation for clinically localized prostate cancer?," *Tech. Urol.* **7**, pp. 12–19, 2001.
4. J. Blasko, T. Mate, J. Sylvester, P. Grimm, and W. Cavanagh, "Brachytherapy for carcinoma of the prostate: Techniques, patient selection, and clinical outcomes," *Seminal Radiation Oncology* **12**, pp. 81–94, 2003.
5. S. Nag, J. Ciezki, R. Cormack, S. Doggett, K. DeWyngaert, G. Edmundson, R. Stock, N. Stone, Y. Yu, and M. Zelefsky, "Intraoperative planning and evaluation of permanent prostate brachytherapy: Report of the american brachytherapy society," *Int. J. Radiat. Oncol., Biol. Phys.* **51**, pp. 1422–1430, 2001.

6. R. Hofstetter, M. Slomezykowski, M. Sati, and L. Nolte, "Fluoroscopy as an imaging means for computer-assisted surgical navigation," *Comput. Aided Surg.* **4**, pp. 65–76, 1999.
7. T. Tang, "Calibration and point-based registration of fluoroscope images," Master's thesis, Queen's University, 1999.
8. J. Yao, R. Taylor, R. Goldberg, R. Kumar, A. Bzostek, R. Vorhis, and P. Kazanzides, "Conic reconstruction and correspondence from two views," *Computer Aided Surgery* **5**, pp. 373–390, 2001.
9. A. Jain, R. Kyon, Y. Zhou, and G. Fichtinger, "C-arm calibration - is it really necessary?," *MICCAI*, pp. 639–646, 2005.
10. Brainlab, Inc., Heimstetten, Germany, *Vector Vision*.
11. Medtronic Surgical Navigation Technologies, Louisville, CO., *StealthStation*.
12. GE Healthcare, Waukesha, WI, *OEC 9800 FluoroTrak*.
13. R. Phillips, A. Mohsen, W. Viant, S. Malek, Q. Li, N. Shah, M. Bielby, and K. Sherman, "A phantom based approach to fluoroscopic navigation for orthopaedic surgery," *MICCAI*, pp. 621–628, 2004.
14. A. Jain, T. Mustafa, Y. Zhou, C. Burdette, G. Chirkjian, and G. Fichtinger, "Ftrac - a robust fluoroscope tracking fiducial," **32**, pp. 3185–3198, 2005.
15. A. Jain, Y. Zhou, T. Mustafa, C. Burdette, G. Chirikjian, and G. Fichtinger, "Matching and reconstruction of brachytherapy seeds using the hungarian algorithm," **32**, pp. 3475–92, 2005.
16. J. Wright, A. Wagner, S. Rao, and Y. Ma, "Homography from coplanar ellipses with application to forensic blood splatter reconstruction," *cvpr* **1**, pp. 1250–1257, 2006.
17. P. K. Mudigonda, C. V. Jawahar, and P. J. Narayanan, "Geometric structure computation from conics," *Lancet. Oncol.* **4**, pp. 233–241, 2002.
18. L. Quan, "Conic reconstruction and correspondence from two views," *IEEE-PAMi* **18**, 1996.
19. F. Kahl and A. Heyden, "Using conic correspondence in two images to estimate the epipolar geometry," in *ICCV*, pp. 761–766, 1998.
20. S. D. Ma, "Conics-based stereo, motion estimation, and pose determination," *International Journal of Computer Vision* **10**, pp. 7–25, 1999.
21. A. Fitzgibbon, M. Pilu, and R. B. Fisher, "Direct least square fitting of ellipses," *Pattern Analysis and Machine Intelligence* **21**, pp. 476–480, 1999.
22. E. S. Maini, "Robust ellipse-specific fitting for real-time machine vision," *IEEE Transactions on Pattern Analysis and Machine Intelligence* **25**, pp. 1343–1348, 2003.
23. G. Jiang, H. Tsui, L. Quan, and A. Zisserman, "Geometry of single axis motions using conic fitting," *Lecture notes in computer science* **3704**, pp. 318–327, 2005.
24. R. Hu and Q. Ji, "Camera self-calibration from ellipse correspondences," *Proceedings of the 2001 IEEE International Conference on Robotics and Automation*, 2001.
25. M. S. Costa and L. G. Shapiro, "3d object recognition and pose with relational indexing," *Computer Vision and Image Understanding* **79**, pp. 364–407, 2000.